POAC'23
Glasgow, United Kingdom

Proceedings of the 27th International Conference on
Port and Ocean Engineering under Arctic Conditions
12-16 June 2023, Glasgow, United Kingdom

THE TENSILE STRENGTH OF SEA ICE: REVISING ITS DEPENDENCE ON MICROSTRUCTURE AND GROWTH VELOCITY

Sönke Maus[1]

[1]Dep. of Civil and Transport Engineering, Norwegian University for Science and Technology, Trondheim, NORWAY, email: sonke.maus@sea-ice.no,

ABSTRACT

The dependence of most physical properties of sea ice on its microstructure is not well established. For the tensile strength, several investigators have discussed its dependence on the *plate spacing*, also referred to as *substructure* or *brine layer spacing*. Also brine pore scales and grain size have been suggested as structural properties that influence the tensile strength. However, due to a lack in detailed microstructure observations and the limited tensile strength data, the validation and formulation of a concise model of sea ice tensile strength is still lacking. Here I revise the models once proposed, on the basis of recently available 3D micro-tomographic images of young sea ice and laboratory-grown model ice. Relationships between microstructure scales (plate spacing, characteristic brine pore width, grain size) and growth conditions (growth velocity, brine volume fraction) are compared to observations from the 3D imagery, to propose an equation for the horizontal tensile strength σ of sea ice that is consistent with the majority of published test results. The analysis suggests a strong influence of the plate spacing, and thus of the ice growth rate, as well as the grain size on the tensile strength of sea ice.

KEY WORDS: Sea ice microstructure, salinity, tensile strength, grain size, fracture

INTRODUCTION

The tensile strength, being the maximum stress that a material can sustain when stretched, is a fundamental mechanical property of sea ice. It is relevant for engineering and geophysical problems like the deformation and failure envelope of sea ice on large scales (Weeks, 2010). However, true tensile tests are difficult to set up in the field, while laboratory procedures are time consuming and have to be of high precision with regard to test-setup and specimen preparation. E.g., early studies of the tensile strength of saline ice have shown, that the so-called Brazil test results are difficult to interpret in terms of the intrinsic tensile strength (Assur, 1958; Weeks, 1961). Observations of the tensile strength of sea ice are thus sparse, and our understanding of sea ice in tension is still incomplete.

Tensile strength tests have been performed for saline laboratory ice, first-year and multi-year sea ice (Timco and Weeks, 2010). The tensile strength tests of young saline ice and first-year sea ice may be divided into laboratory (Dykins, 1970; Kuehn and Schulson, 1994; Richter-Menge and Jones, 1993) and field tests (Dempsey et al., 1999, 2018). All studies have in common that they show a strong dependence of tensile failure loads on brine porosity. That field scale tests give smaller load for tensile failure has been attributed to two types of size effects - an energetic one on the basis of linear elastic fracture mechanics and a statistic one based on the view that larger sea ice specimen contain larger flaws (Dempsey et al., 1999; Dempsey, 2000). What is currently lacking for all scales are observations and models of failure generating flaws and microstructure.

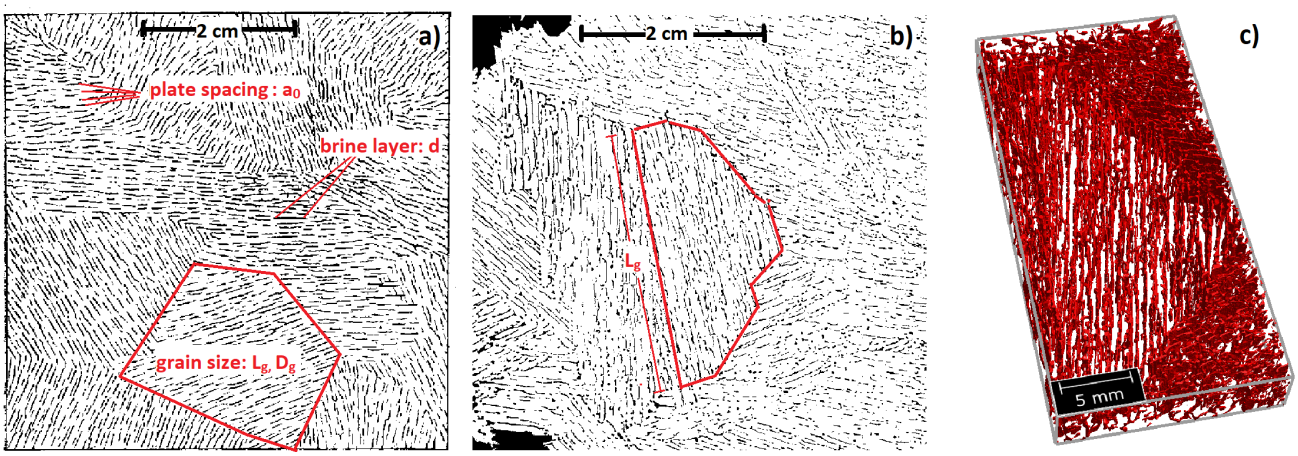

Figure 1: Ilustration of basic scales of sea ice microstructure: brine layer width d, plate spacing a_0 and grain size (with equivalent grain diameter D_g and grain length L_g in the direction of brine layers). a) thinfoil replica from the bottom of sea ice (Drygalski, 1897); b) horizontal X-ray tomographic slice from the skeletal layer of young sea ice; c) enlarged 3D version (43 x 17 x 4 mm) of the central grain in b). Ice and pores are white/back (a, b) or invisible/red (c).

The present paper deals with the small-scale (plastic limit) tensile strength of columnar sea ice under horizontal loading. This is done on the basis of an approach to predict the dependence of the tensile strength of sea ice on its microstructure and porosity formulated half a century ago (Anderson and Weeks, 1958; Weeks and Assur, 1964). This approach will be revised on the basis of recent modelling and observations of sea ice microstructure. The revised model proposed here for the horizontal tensile strength of sea ice takes into account three characteristic microstructure length scales of sea ice shown in Fig. 1. These are the lamellar or plate spacing a_0, the width d of brine layers or pores between the plates, and the grain dimensions. Grains can be identified in terms of c-axis orientation and appear in horizontal thin sections as pattern with parallel plates and brine layers. They are often elongated in one direction, and may for horizontal sections be characterised by an equivalent grain diameter D_g (square root of grain area A_g) and the length L_g of its major axis (parallel to the brine layers).[1]

MICROSTRUCTURE-BASED STRENGTH MODELLING

Several authors have discussed the relationship between strength, microstructure and porosity (Anderson and Weeks, 1958; Assur, 1958; Weeks and Assur, 1964) based on the approach

$$\sigma = \sigma_0(1 - \chi), \tag{1}$$

where χ is the reduction in the cross-sectional strength bearing area. The first assumption is that, due to the lamellar structure of sea ice, $\chi = 1$ as long as the microstructure is dominated by columnar planar brine layers, the horizontal tensile strength is zero. Furthermore, if the planar brine layers simply become thinner with decreasing porosity the strength will remain zero. First when ice bridges form within the planar brine layers the sea ice gains strength. The strength evolution will then depend on the geometry of ice bridges and their evolution, and different models have been proposed and discussed (Anderson and Weeks, 1958; Assur, 1958; Weeks and Ackley, 1986; Richter-Menge and Jones, 1993). To quantify the strength reduction in Eq. 1 the following two microstructure evolution models are considered.

The most frequently discussed microstructure-strength model is illustrated in Fig. 2. It is assumed that brine layers split into vertical cylinders at critical brine layer thickness d_0. Strength is established when these vertical cylinders detach as shown in the figure. The second model considers splitting at d_0 into rectangular sheets or columns (not in the figure). The strength reduction for these two models may be computed as follows:

[1]Note that the grains are much longer in the (vertical) direction of columns.

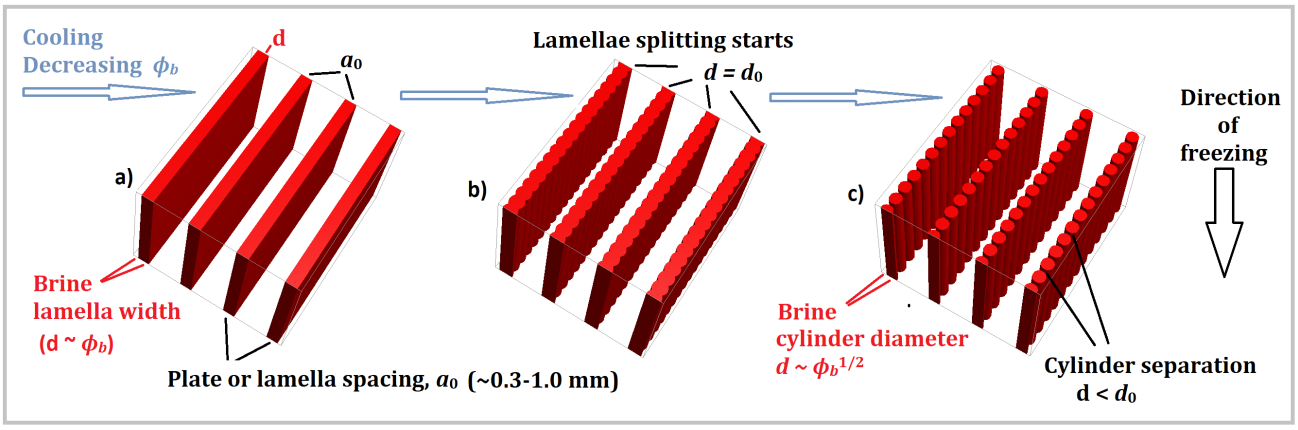

Figure 2: Schematic of the microstructure evolution during cooling of columnar sea ice as first proposed by Anderson and Weeks (1958). Brine is shown in red, with ice being invisible. During cooling from a) to c) the brine volume fraction ϕ_b decreases: a) brine layer thickness d changes linearly with brine volume fraction ϕ_b; b) at $d = d_0$ brine layers start splitting into cylinders; c) brine lamellae are split into cylinders that no longer touch each other and ice necks have formed establishing the strength; now the cylinder diameters shrink according to $d \sim \phi_b^{1/2}$.

Splitting into circular cylinders. The zero strength brine volume ϕ_{b0} is

$$\phi_{b0} = \frac{\pi d_0}{4a_0}, \tag{2}$$

where a_0 is the spacing of circular brine layers (also called plate spacing). After splitting at d_0 and ϕ_{b0} the diameter d shrinks with the square root of the brine volume further according to

$$d = \phi_b a_0, \qquad \phi_b > d_0/a_0 \tag{3}$$
$$d = d_0, \qquad \phi_{b0} < \phi_b < d_0/a_0 \tag{4}$$
$$d = d_0(\phi_b/\phi_{b0})^{1/2}, \qquad \phi_b < \pi d_0/4a_0 \tag{5}$$

This gives the strength reduction as

$$\sigma = \sigma_0 \left(1 - \frac{d}{d_0}\right). \tag{6}$$

which using Eq. 2 may be written as

$$\sigma = \sigma_0 \left(1 - \left(\frac{4a_0\phi_b}{\pi d_0}\right)^{1/2}\right). \tag{7}$$

Splitting into rectangular columns. The critical brine volume fraction is then

$$\phi_{b0*} = \frac{d_0}{a_0}. \tag{8}$$

It is assumed that the columns keep their thickness d_0 and only shrink in the plane of brine layers:

$$d = \phi_b a_0, \qquad \phi_b > d_0/a_0 \tag{9}$$
$$d = d_0, \qquad \phi_b < d_0/a_0 \tag{10}$$

This implies a strength reduction that is linearily proportional to the brine volume

$$\sigma = \sigma_0 \left(1 - \frac{\phi_b}{\phi_{b0*}}\right) = \sigma_0 \left(1 - \frac{a_0\phi_b}{d_0}\right). \tag{11}$$

In addition to the square root and linear dependence of σ on the brine volume, a model may involve more structural parameters like the vertical splitting and shrinking behaviour of brine cylinders as well as elliptical pores (Assur, 1958; Weeks and Assur, 1964). Richter-Menge and Jones (1993) have suggested an equation that mixes the linear and square-root dependencies. However, due to a lack in microstructure data such approaches have remained unvalidated.

Plate spacing and brine layer splitting

The sea ice strength based on Eq. 7 and 11 depends essentially on the ratio d_0/a_0 of two microstructure scales. Anderson and Weeks (1958) were the first to estimate these scales. For the plate spacing a_0 they obtained a value of 0.46 mm from 50 measurements on photographs of sea ice from many conditions. They further reported that elliptical inclusions just after splitting of brine layers had a short dimension of 0.07 mm. Based on these observations Anderson and Weeks (1958) proposed that ϕ_{b0} takes the constant value $d_0/a_0 = 0.07/0.46 = 0.152$, representing the critical brine volume below which the tensile strength of sea ice will approach zero.

Weeks and Assur (1964) estimate d_0 indirectly by determination of ϕ_0 and a_0. They did so by grouping the ring tensile strength data from Weeks (1961) into depth intervals, for which a_0 was estimated from an empirical relationship, and ϕ_{b0} by least squares. Inserting these values into Eq. 10 a best fit of $d_0 = 0.112 \pm 0.01$mm was obtained, much larger than the $d_0 = 0.07$ mm value proposed by Anderson and Weeks (1958). This has been regarded as a major discrepancy to model strength on the basis of microstructure observations. A recent analysis of a large dataset of micro-tomographic imagery (Maus et al., 2021) has shed new light on this topic. In that study the permeability threshold was associated with a characteristic bottleneck or throat diameter/width of 0.07 ± 0.01 mm, while the median pore diameter of all connected pores was 0.12 ± 0.01 mm at the threshold. This result explains the noted discrepancy between the studies by Anderson and Weeks (1958) and Weeks and Assur (1964) in that shows that the diameter of a pore at a splitting location (≈ 0.07mm) differs from the average diameter of pores (≈ 0.12mm). It is the latter average diameter that needs to be used in connection with the average brine volume and the relationship to sea ice strength. In the present model I shall assume that $d_0 = 0.12$ mm is a constant.

The pore space analysis by Maus et al. (2021) has revealed another important aspect of the present strength model approach. For the porosity range 0.03 to 0.20 the minor pore dimension was changing according to a power law $d \sim \phi_b^e$ with an exponent $e = 0.34 \pm 0.05$ for pores and 0.46 ± 0.06 for throats. This indicates that the square root model is much more consistent with microstructure observations.

Due to the challenges to observe a_0 and in particular d_0 most investigators have determined the critical ϕ_{b0} by a least squares fit of strength versus brine volume $\phi_b^{1/2}$. Extensive data were obtained with the ring tensile strength test and, though this is no longer considered as a valid tensile strength test for sea ice, the range of ϕ_{b0} obtained is of interest. Assur (1958) found an average $\phi_{b0} \approx 0.15$, yet they also showed, for three data sets, a range $0.13 < \phi_{b0} < 0.20$, with higher values for ice with higher salinity. Weeks (1961) obtained $\phi_{b0} \approx 0.231$ from a large set of ring-tensile tests of laboratory-grown NaCl ice. Based on 1470 test results Frankenstein (1969) gave almost the same $\phi_{b0} \approx 0.233$. If one considers also flexural and compressive strength tests, a wide range $0.1 < \phi_{b0} < 0.3$ has been found for the $\phi_{1/2}$ model (Schwarz and Weeks, 1977; Zhan et al., 1996; Timco and Weeks, 2010). In some studies investigators have correlated strength with the total (brine and air porosity) which gives a higher threshold. The highest $\phi_{b0} = 0.32$ was derived from the relationship of compressive strength and total (air and brine) porosity of warm first-years ice (Timco and Frederking, 1986), while the lowest value so far ($\phi_{b0} = 0.08$) was reported by Sammonds et al. (1998) for multiyear sea ice.

Based on the above review it is obvious that ϕ_{b0} is quite variable, and if d_0 is assumed constant, this variability must be related to variations in a_0. Indeed, it is well known that a_0 is not constant (Weeks, 2010; Shokr and Sinha, 2015) and the increase of a_0 with ice thickness was also an important aspect of the above-mentioned study by Weeks and Assur (1964). A recent study by the author (Maus, 2020) has demonstrated that the plate spacing a_0 may be predicted on the basis of morphological stability theory (Mullins and Sekerka, 1964) in dependence on the ice growth velocity in the form

$$a_0 = 0.72 V^{-1/3}, \tag{12}$$

where a_0 is in millimetres and V in cm/day. The equation is valid for ice grown uni-directionally from seawater or NaCl solutions with similar salinity, and for growth velocities below 15 cm/day.[2]

[2]At higher V, due to absence of solutal convection, a relationship with an exponent $-2/3$ is observed and predicted.

Predicted bounds on tensile strength of saline ice

In summary, there are two important length scales in young saline ice. The first is the width or diameter d of brine channels between the ice lamellae. It is not constant yet changing with porosity (with salinity and temperature), and upon reaching a critical width d_0 the brine lamellae separate into cylinders. According to our present knowledge d_0 may be assumed constant and ≈ 0.12 mm. The second is the plate spacing a_0 that decreases with growth velocity. With the growth velocity of natural sea ice in the range $0.4 < V < 15$ cm/day Eq. 12 predicts a plate spacing range off $1.0 > a_0 > 0.3$ mm which is consistent with a large set of laboratory and field studies (Maus, 2020). Inserting this range into Eq.s 7 and 11 gives the expected range in the tensile strength, normalised by the zero porosity limit, shown in Fig. 3. According to the model one can expect a very strong dependence of the tensile strength on the plate spacing, with a zero strength porosity that varies from $\phi_{b0} \approx 0.1$ for slowly growing sea ice with large a_0 to 0.3 for rapidly growing young ice.

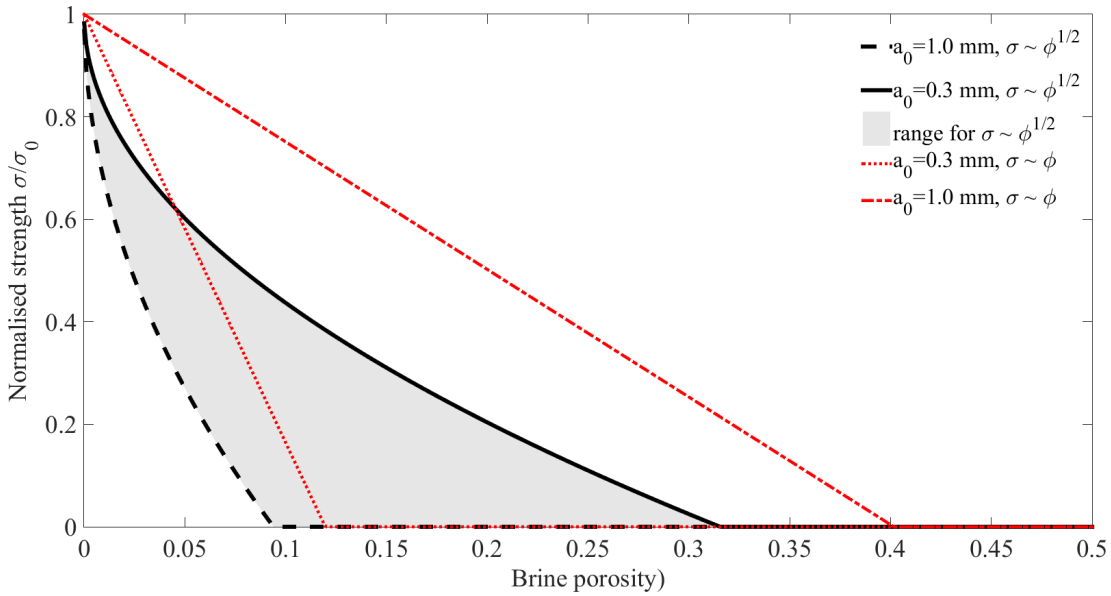

Figure 3: Normalised strength based on the square root and linear models of brine pore evolution. Both models are shown for $d_0 = 0.12$mm and the bounds $0.3 < a_0 < 1.0$mm in the plate spacing, corresponding to the range $0.4 < V < 15$ cm/day in the growth velocity. The range for the square root model is shown in grey shading.

Ice thickness and growth velocity

To compare the model to observations plate spacing data are needed. The latter has seldom been measured in sufficient detail in strength test specimen - except in the study by Dykins (1967, 1969). However, ice growth velocity can often be estimated from documented growth conditions, which then enables to estimate a_0 with Eq. 12. In the absence of detailed meteorological observations

$$H^2 + \frac{2K_i}{C_t}H = \frac{2K_i}{\rho_i L}\Theta \tag{13}$$

is a useful model (Maykut, 1986; Petrich and Eicken, 2010). Θ is the time integral of the difference of air temperature T_a and water freezing point T_f (often approximated as cumulative freezing degree days). L and ρ_i are the latent heat of fusion and density of sea ice, K_i thermal conductivity, C_t the heat transfer coefficient at the ice-air interface. The corresponding ice growth velocity becomes

$$V = \frac{K_i}{H}\left(1 + \frac{K_i}{C_t H}\right)^{-1}\frac{T_a - T_f}{\rho_i L}. \tag{14}$$

The effect of snow may be included in asimple manner, assuming that snow thickness is proportional to ice thickness ($H_s = \alpha H$). This leads to a solution where one replaces K_i by $K_i/(1 + \alpha K_i/K_s)$,

where K_i/K_s is the ratio of thermal conductivities of ice and snow. Here I have these equations with thermo-physical properties $K_i = 2.04$ Wm^{-1}K^{-1} $L\rho_i = 304$ kJ m^{-1} accounting for 0.1 brine volume, , $C_t = 24$ Wm^{-1}K^{-1} and $K_i/K_s = 7$ similar to values proposed by (Maykut, 1986).

Overview of tensile strength data with microstructure

The published data from three tensile strength studies of sea ice (from the field and laboratory tank studies) will be compared to the present model. Test conditions and average strength test results are given in Table 1 and described as follows, focusing in particular on the ice growth velocities.

Dykins (1967, 1969, 1970)–DYK. The experiment was performed in an indoor tank with 1.6 x 2.6 m surface exposure, where the ice grew to 56 cm thickness before test specimen were extracted. Room temperatures were cycling between -15 to -20°C, with fans persistently enhancing the heat exchange over the ice. During ice growth to 56 cm the water salinity increased to $\approx$ 60 ‰, yet strength data were obtained only for the levels 4-40 cm for which the salinity likely was between 32.5 and 53 ‰. The strain rate estimated from stress divided by elastic modulus (Richter-Menge and Jones, 1993) was in the range 2-5$\times 10^{-5}$ s^{-1}, test specimen has a diameter of 4.05 cm. The grain size was increasing from 3-5 mm near the surface (3 cm depth) to 14 mm at 40 cm depth. The corresponding plate spacing at these levels was increasing from 0.3-0.4 mm near to 0.4-0.5 mm. at 40 cm depth in the ice, and the growth velocity range 4 to 9 cm/day has been estimated based on the observations, lower values near the bottom. Using the same growth law as for the field one would obtain a near-surface growth velocity consistent with this estimate, yet the near-bottom value would be smaller. A possible explanation for this discrepancy could be lateral heat loss from the ice in spite of lateral insulation.

Kuehn et al. (1990)–KUE. Saline ice was grown from "Instant Ocean" water of salinity 20 ‰ in a laboratory tank of 91.4 cm diameter and 121.9 cm depth. The tank was placed in a cold room at 0 °C with a cooling plate on top. The ice growth was reported as 30 to 60 cm in 2 to three weeks. In addition to salinity, density and grain size, also the vertical column length was documented as 5-17 cm. Tests were performed at strain rates of 10^{-3} and 10^{-7} s^{-1} on 25-30 cm long cylinders of 10 cm diameter. However, the location (vertical) of the cylindrical specimen was not documented, and the ice properties in Table 1 thus just refer to the core averages given. The typical growth velocity range 1 to 3 cm/day may be estimated with Eq. 14 for the levels 5 and 55 cm, assuming $T_a = -10$ °C as documented by Kuehn and Schulson (1994). To predict similar ice as reported for this setup requires $C_t \approx 17$ Wm^{-1}K^{-1}, which is smaller than normally observed in the field. A plausible explanation is that a cooling plate on top of the tank limits the convective heat transfer over the ice surface.

Richter-Menge and Jones (1993)–RMJ. Natural sea ice samples were obtained from 4 levels of ice from a 166 cm thick refrozen lead in the Alaskan Beaufort Sea, for which grain size, salinity and density were documented. Ocean water salinity was likely between 30 and 32 during winter in the Beaufort Sea coastal areas. Tests were performed at the temperatures -3, -5, -10 and -20 °C, with the lowest temperature for surface ice samples, increasing downwards in order to be close to in situ conditions. Tests were performed at strain rates of 10^{-3} and 10^{-5} s^{-1} on 25 cm long samples with 10 cm diameter. The plate spacing was not determined in detail, yet the range 0.5 to 1.0 mm was noted. Growth history of this refrozen lead ice has not been documented, yet we estimate growth rates at the depth levels corresponding to test groups. To do so we use the growth model Eq. 14, and assume upper and lower bounds corresponding to $Ta = -30$ °C, snow thickness 1/20 of ice thickness, as well as $T_a = -20$°C, snow thickness 1/10 of ice thickness.

Among the many properties in the table the difference in plate spacings between the different studies is considered most important. For the DYK data the range 0.3-0.6 mm is reported for the plate spacing, compared to 0.5-1.0 mm for KUE and RJM. While Dykins obtained an average a_0, as well as its variation with depth, KUE and RMJ did not provide such information. However, considering the growth conditions it is possible to estimate the plate spacing for the ice from KUE and RMJ. Hence, as a principle difference between the experiments it turns out that the strength tests from DYK were performed on ice growing with higher velocity (4-9 cm/day), and smaller plate spacing (0.35-0.45 mm) when compared to the ice from KUE and RMJ (for which 0.6 to 3 cm/day and 0.5-0.85 mm).

Strain rate s^{-1}	Z_i m	T °C	S ‰	ρ kgm^{-3}	$\phi_b^{1)}$ %	$\phi_a^{1)}$ %	$a_0^{2)}$ mm	$V^{3)}$ cm/day	D_g mm	σ_t MPa
Dykins (1967): Laboratory ice, H_i = 56 cm, initial $S_w = 32.54$, 0.3 < a_0 < 0.6 mm										
2-5×10^{-5}	0.05-0.4	-27	8.4	926	1.0	0.08	0.35-0.45	4-9	3-14	0.55 ± 0.03
2-5×10^{-5}	0.05-0.4	-20	8.5	927	2.86	0.06	0.35-0.45	4-9	3-14	0.47 ± 0.03
2-5×10^{-5}	0.05-0.4	-10	7.6	910	4.15	1.81	0.35-0.45	4-9	3-14	0.47 ± 0.02
2-5×10^{-5}	0.05-0.4	-4	5.3	876	6.15	5.43	0.35-0.45	4-9	3-14	0.29 ± 0.02
Kuehn et al. (1990): Laboratory ice, H_i = 30 cm, initial $S_w = 20$, 0.5 < a_0 < 1.0 mm										
10^{-3}	0.05-0.55	-10	4.3	914	2.4	1.0	0.50-0.72	1-3	1.6-5.2	0.35 ± 0.15
Richter-Menge and Jones (1993). Field ice, H_i = 166 cm, $S_w \approx 30 - 32$, 0.5 < a_0 < 1.0 mm										
10^{-3}	≈ 0.2	-20	5.6	922	1.9	0.3	0.41-0.49	3.1-5.5	2.3-4.2	0.78 ± 0.14
10^{-5}	≈ 0.2	-20	5.4	925	1.8	0.0	0.41-0.49	3.1-5.5	2.3-4.2	0.73 ± 0.07
10^{-3}	≈ 0.7	-10	4.1	919	2.3	0.4	0.58-0.72	1.0-1.9	3.5-4.4	0.63 ± 0.12
10^{-5}	≈ 0.7	-10	4.1	918	2.3	0.5	0.58-0.72	1.0-1.9	3.5-4.4	0.56 ± 0.06
10^{-3}	≈ 1.1	-5	3.5	919	3.5	0.4	0.66-0.81	0.7-1.3	3.3-4.4	0.47 ± 0.13
10^{-5}	≈ 1.1	-5	3.3	916	3.3	0.7	0.66-0.81	0.7-1.3	3.3-4.4	0.45 ± 0.06
10^{-3}	≈ 1.3	-3	2.9	913	4.6	1.1	0.70-0.85	0.6-1.1	5.4	0.31 ± 0.06
10^{-5}	≈ 1.3	-3	3.1	912	5.0	1.2	0.70-0.85	0.6-1.1	5.4	0.21 ± 0.09

Table 1: Summary of tensile strength data from Dykins (1967)–DYK, Richter-Menge and Jones (1993)–RMJ and Kuehn et al. (1990)–KUE: Z_i is level in the ice measured from top, T ice temperature, S salinity, ρ density, ϕ_b and ϕ_a brine and air porosity, a_0 plate spacing, V ice growth velocity, D_g equivalent grain size, σ tensile strength. Footnotes: $^{1)}$ computed from density, temperature and salinity according to Cox and Weeks (1983); $^{2)}$ observed in DYK, estimated from growth velocity for RMJ and KUE; $^{3)}$ estimated from a_0 for DYK; estimated from ice growth equation for RMJ and KUE;

Tensile strength σ_0 at low porosity:

To predict the tensile strength via Eq.s 11 and 7 one also needs to know the tensile strength σ_0 at low porosity. As noted above, most researchers have obtained σ_0 from least square fits of Eq.s 11 or 7. However, with the indicated range based on a_0 and the model type (linear versus square root) such fits are very uncertain. Here I suggest a different approach, on the basis of tensile strength studies of fresh-water ice, showing a grain-size dependent tensile strength related to the nucleation and propagation of cracks (Michel, 1978a,b; Currier and Schulson, 1982; Lee and Schulson, 1988; Kolari, 2017). For sea ice, with many pre-existing cracks, I assume that fracture is dominated by crack propagation, and that the tensile strength can be approximated as

$$\sigma_0 = K_{Ic} \left(\frac{4}{\pi} R \right)^{-1/2}, \tag{15}$$

where K_{Ic} is the fracture toughness and R is the radius of a penny-shaped crack. This crack should be associated with the largest brine inclusions in the original brine layers. While observations of such pattern are generally sparse, Eicken et al. (2000) have provided some useful data. These authors obtained the major and minor axis length in vertical and horizontal thin sections for natural and laboratory-grown sea ice. The maximum vertical and horizontal major axis lengths of brine inclusions were in the range 3 to 5 mm. Though the detailed 3D morphology was not determined, the largest pattern appear to be brine patches with dimensions similar to the grain size (for which 5-10 mm can be estimated).

To obtain a better idea of these brine pattern, I have analysed imagery from a 3D X-ray tomographic data set that recently was used to simulate the permeability of sea ice Maus et al. (2021). In Fig. 4 the microstructure is shown in three ways, and for three temperatures and corresponding brine porosities shown in rows a) to c). The left hand side shows a 3D view of the pore space. The middle image shows a horizontal section, with brine layers being clearly defined at high porosity and temperature. The right hand images shows vertical sections viewed in the plane of the brine layers. It is seen that, for all temperatures and brine volume fractions, there exist patches with high brine coverage with dimensions 5 to 10 mm. The equivalent grain size of this young ice was in the range 5 to 9 mm.

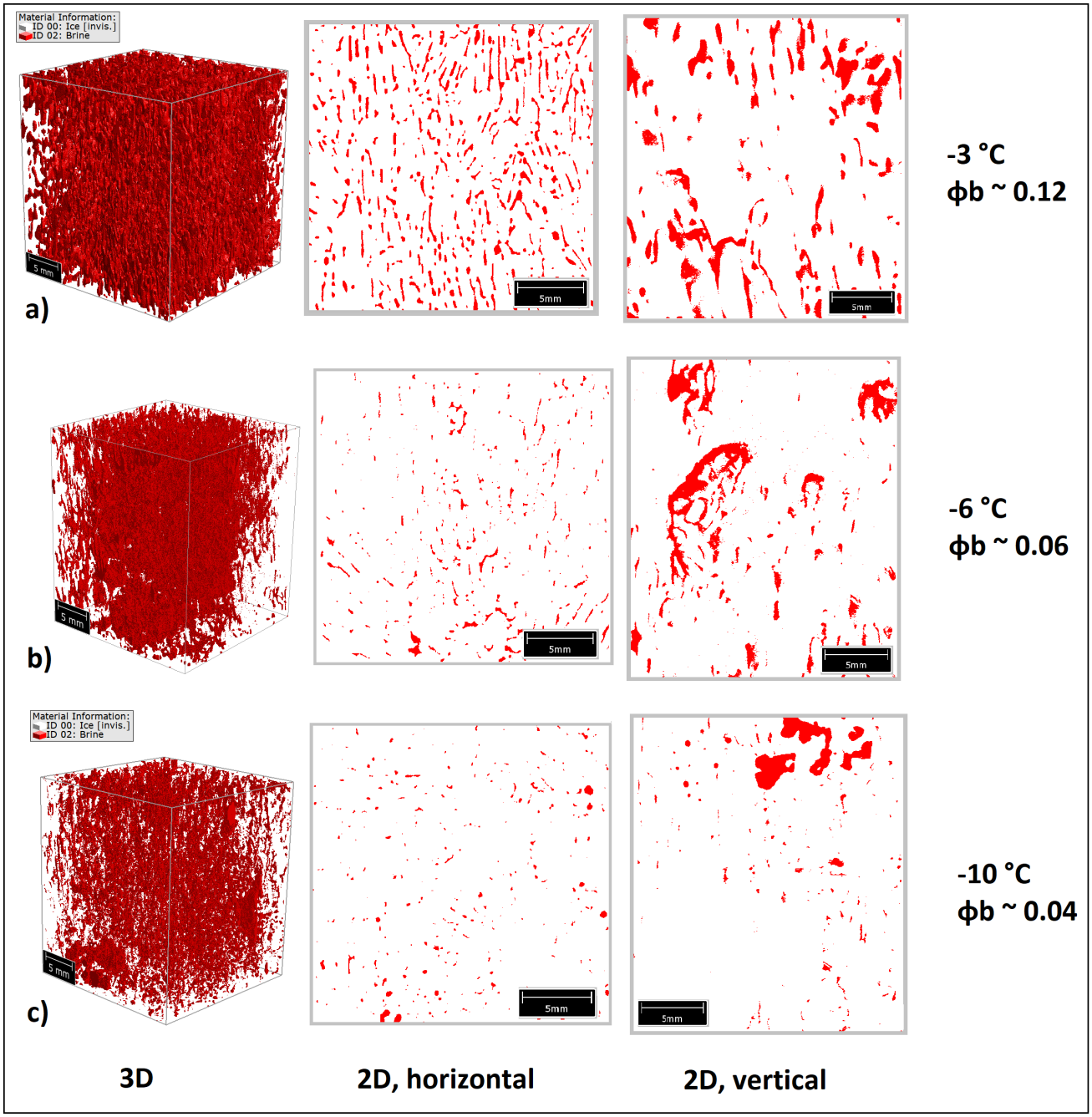

Figure 4: Brine pore space of young sea at three temperatures and corresponding brine porosities in rows a) to c). Left: 3D view of the pores space; mid: horizontal section with brine layers clearly visible in a); right: vertical sections viewing the pores in a brine layer plane.

Hence, there exist high porosity patches of similar or even larger size than the equivalent grain size D_g. Would then D_g be the right length scale to be associated with the crack diameter $2R$ in Eq. 15? With largest inclusions located in the planes of original brine layers, one would expect that the length L_g of grains is more relevant. As the grain size is mostly reported as an equivalent diameter D_g, also for the studies in Table 1, how large is L_g? With the definitions from the introduction that $D_g \approx A_g^{1/2} \approx (L_g W_g)^{1/2}$, where A_g is grain area and L_g and W_g are grain length and width. This can be written as $L_g/D_g \approx (L_g/W_g)^{1/2}$. Weeks and Ackley (1986) show measurements (their figure 31) of L_g versus W_g for ice from Thule, Greenland, with the ratio L_g/W_g between one and 6. Shokr and Sinha (2015) report an average L_g/W_g of 2.7 for the surface of second-year ice (their Figure 4.48), while Weeks and Hamilton (1962) measured a ratio from 1 to 3 with an average of 2 for young ice. This brief review indicates that the average $L_g/D_g \approx (L_g/W_g)^{1/2}$ is in the range $2^{1/2} - 3^{1/2}$, while maxima are from $3^{1/2} - 6^{1/2}$. In the following 2 is used to convert from grain size D_g to length L_g.

DISCUSSION

Based on the microstructure review the model proposed for the horizontal tensile strength is

$$\sigma = K_{IC} \left(\frac{2}{\pi} L_g\right)^{-1/2} \left(1 - \left(\frac{4 a_0 \phi_b}{\pi d_0}\right)^{1/2}\right). \tag{16}$$

Note that a similar strength parametrisation, yet with constant ϕ_{b0} instead of a_0 and d_0, was proposed by Michel (1978b,a). To compared it to the observations in Table 1 we use $K_{IC} = 0.1$ MPa m$^{1/2}$ for the fracture toughness, a grain L_g two times the observed D_g, the typical range for the plate spacing a_0, a critical brine layer width of $d_0 = 0.12$ mm. Then the tensile strength becomes a function of the brine porosity ϕ_b.

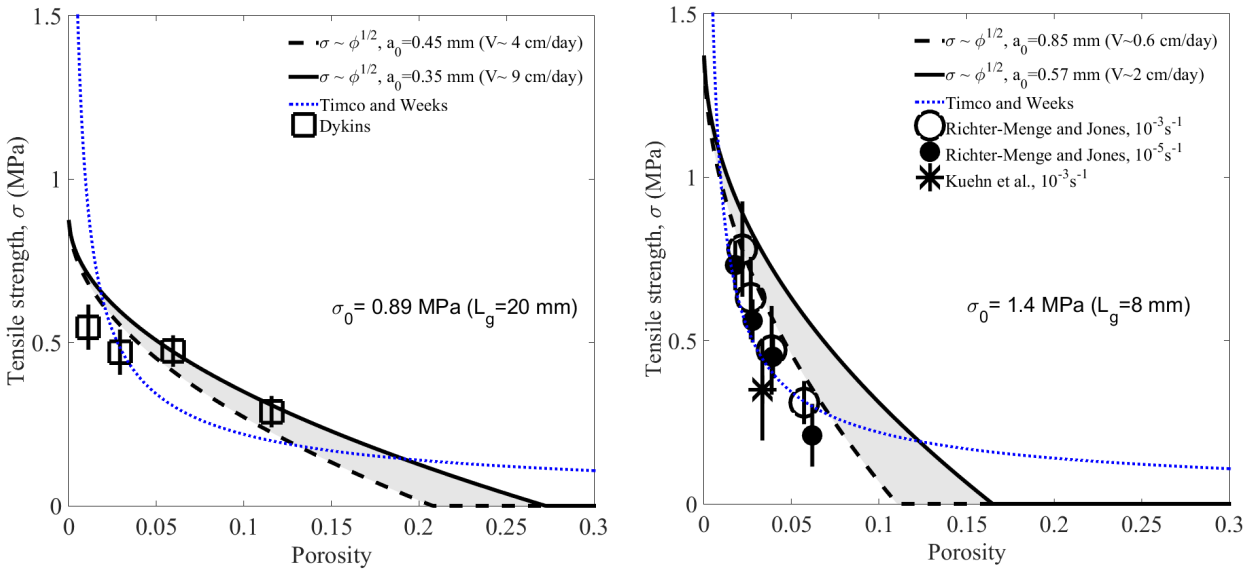

Figure 5: Modeled (Eq. 16) versus observed tensile strength: a) Observations from Dykins (1967) versus model predictions for $0.35 < a_0 < 0.45$ mm and $L_g = 20$ mm; b) observations from Richter-Menge and Jones (1993) and Kuehn et al. (1990) versus model predictions for $0.57 < a_0 < 0.85$ mm and $L_g = 8$ mm, typical for their sea ice growth conditions (see Table 1). Observations are shown with total (air plus brine) porosity.

Fig. 5a and b compares the model predictions versus the strength test results from DYK to those from RMJ with one average data point from KUE. The main difference in the microstructure is the smaller plate spacing and larger grain size in a) compared to b), and model ranges are shown to account for this difference. The model captures the different trends in the two data sets rather well. The smaller slope in the DYK data is related to higher ϕ_{b0} (due to smaller plate spacing) and smaller σ_0 (due to larger grain size). The steeper increase of strength with decreasing porosity as shown by the data from RMJ can be explained by smaller ϕ_{b0} (larger plate spacing) and larger σ_0 (due to smaller grain size).

For the DYK ice the model approach predicts, with a representative range $0.35 < a_0 < 0.45$mm and $L_g = 20$ mm, $\sigma_0 = 0.89$ MPa and ϕ_{b0} in the range 0.21-0.27. For the RMJ and KUE ice we have taken $L_g = 8$ mm and a representative growth velocity regime of 0.6-2 cm/day which gives $0.57 < a_0 < 0.85$ mm as typical range. Eq. 16 and 2 then give $\sigma_0 = 1.40$ MPa and ϕ_{b0} in the range 0.11 to 0.17. We can compare these numbers to earlier results based on least square fitting of σ versus ϕ_b. Dykins himself had obtained $\sigma_0 = 0.82$ MPa and $\phi_{b0} = 0.142$, on the basis of averaging at the four temperatures given in Table 1, yet for fitting strength versus brine porosity only. RMJ analysed all individual data points from Dykins, and obtained a lower $\phi_{b0} = 0.095$ as well as $\sigma_0 = 1.11$ MPa when correlating strength with total porosity. For their own test data RMJ obtained, with the square root model, σ_0 in the range 1.46 to 1.83 MPa (dependent on strain rate) as well as ϕ_{b0} in range 0.064-0.074.

Overall, the present strength model gives similar numerical values for σ_0, yet larger ϕ_{b0}, than obtained from least square fits. Its novelty is that it is based on first principles and observed and

modelled microstructure, and gives plausible explanations for the difference in the porosity-strength relationships for the ice from DYK and RMJ, in terms of plate spacing and grain size. In Fig. 5a and b we also show the equation $\sigma = 4.278\phi^{-0.6455}$ proposed by Timco and Weeks (2010) on the basis of the data from Table 1, with σ in MPa and the porosity in ‰. While predicting some of the data, it does not capture the microstructure-based relationships proposed in the present work.

For the tensile strength predictions in Fig. 5 most plausible properties for the microstructure were used in Eq. 16 finding good agreement with observations. No attempt is made here to tune this agreement further, yet some principle uncertainties of properties can be discussed. The fracture toughness $K_{IC} = 0.1$ MPa m$^{1/2}$ assumed is representative for ice and sea ice, for which most studies have determined values in the range 0.07 to 0.15 MPa m$^{1/2}$ (Dempsey, 1991). A 20 % smaller value than used here would bring the RMJ observations and predictions into closer agreement. A 40 % higher L_g would have a similar effect. As grain size estimates are mostly based on counting grains, they are dominated by small grains, while the longest grains contain the largest brine pattern leading to failure. Hence, larger L_g is plausible. For the critical brine layer thickness d_0 of 0.12 mm little data exist, and the uncertainty of the estimate from Maus et al. (2021) is 0.01 mm. With a 10 % uncertainty in a_0 (Maus et al., 2021), the uncertainty in d_0/a_0, and thus ϕ_{b0}, would be $\approx$ 20 %, which translates to 10 % strength uncertainty. Another aspect is that the model agrees much better with observations when plotting strength versus total rather than brine porosity. The argument to do so is that brine that is lost during specimen handling needs to be included as air pore space. However, some pre-existing air pores may affect strength differently.

The present model idealises the pore evolution during cooling/freezing, and assumes that there is no hysteresis during warming. In reality, when ice is warmed again, not all pores reconnect, some of them grow while others stay small, and a certain fraction of porosity remains closed (Maus et al., 2021). This could explain that one seldom observes zero strength at high porosity (Frankenstein, 1969) and may justify an equation as proposed by Timco and Weeks (2010) and shown in Fig. 5. To account for this one would have to introduce additional parameters from microstructure observations. One may also expect that the pore space evolution follows a combination of a square root and linear model, as discussed by Assur (1958) and Richter-Menge and Jones (1993). Microstructure changes during transport and storage of ice cores, at other temperatures than in the field, may also be an issue.

CONCLUSIONS

1. A model has been formulated for the tensile strength σ of sea ice that combines earlier sea ice microstructure models (Assur, 1958; Anderson and Weeks, 1958) with grain-size based strength laws for freshwater ice (Michel, 1978a,b; Lee and Schulson, 1988). It successfully predicts published tensile strength test results.
2. The essential properties in the model are a critical pore size for brine layer splitting d_0, the plate or brine layer spacing a_0, the horizontal major axis length of sea ice grains in the direction of plates L_g, and the fracture toughness K_{ic}.
3. Schulson and Duval (2009) proposed (their section 10.6.3) that the tensile strength of sea ice is likely related to the propagation of cracks, yet that their nature is less related to grain size, yet more to defects 'made of the collection of pores within the planar arrays that characterize the microstructure of sea ice'. The present interpretation is consistent with the planar array hypothesis. However, here it is further proposed that these defects are indeed related to the length of grains in the direction of the ice lamellae.
4. The model proposed here provides a clear path to analyse and model the tensile strength of sea ice and its dependence on growth conditions and microstructure. It hopefully will help to better understand size-dependent fracture processes and tensile failure on larger scales (Dempsey et al., 1999, 2018).
5. For model improvement and validation better statistics of the 3D microstructure of sea ice pore networks, of grain size (in particular grain length L_g), and of their dependence on ice thickness and age are needed.

REFERENCES

Anderson, D. L., Weeks, W. F., 1958. A theoretical study of sea ice strength. Trans. Amer. Geophys. Union 39, 632–640.

Assur, A., 1958. Composition of sea ice and its tensile strength. In: Arctic Sea Ice. Vol. 598. Proc. Conf.on Arctic Sea Ice, Natl. Acad. Sci., pp. 106–138.

Cox, G. F. N., Weeks, W. F., 1983. Equations for determining the gas and brine volumes of sea ice samples during sampling and storage. J. Glaciol. 32, 371–375.

Currier, J. H., Schulson, E., 1982. The tensile strength of ice as a function of grain size. Acta metall. 30, 1511–1514.

Dempsey, J., 1991. The fracture toughness of ice. In: S.J. Jones, R.H. McKenna, J. T., Jordaan, I. (Eds.), Ice-structure-interaction. Springer-Verlag Berlin, pp. 109–145.

Dempsey, J., Adamson, R. M., Mulmule, S. V., 1999. Scale effects on the in-situ tensile strength and fracture of ice. Part II: First-year sea ice at Resolute, N.W.T. Int. J. Fracture 95, 347–366.

Dempsey, J., Cole, D., Wang, S., 2018. Tensile fracture of a single crack in first-year sea ice. Philosophical Transactions of the Royal Society A: Mathematical, Physical and Engineering Sciences 376, 2017.0346.

Dempsey, J. P., 2000. Research trends in ice mechanics. Int. J. Solids and Struct. 37, 131–153.

Drygalski, E., 1897. Grönlands Eis und sein Vorland. Vol. 1 of Grönland-Expedition der Gesellschaft für Erdkunde zu Berlin 1891-1893. Berlin, Kühl, 555 pp.

Dykins, J., 1970. Ice engineering: tensile properties of sea ice grown in a confined system. NCEL Technical Report R680, Naval Civil Engineering Laboratory, Port Hueneme, CA.

Dykins, J. E., 1967. Tensile properties of sea ice grown in a confined system. In: Physics of Snow and ice. Vol. 1. Hokkaido University, Sapporo, Japan, pp. 523–537.

Dykins, J. E., 1969. Tensile and flexure properties of saline ice. In: Physics of ice. 3rd International Symposium on the Physics of Ice, Plenum Press, New York, pp. 251–270.

Eicken, H., Bock, C., Wittig, R., Miller, H., Poertner, H.-O., 2000. Magnetic resonance imaging of sea-ice pore fluids: methods and thermal evolution of pore microstructure. Cold Reg. Sci. Techn. 31, 207–225.

Frankenstein, G. E., 1969. Ring tensile strength studies of ice. Crrel research report 172, Cold Regions Research and Engineering Laboratory.

Kolari, K., 2017. A complete three-dimensional continuum model of wing-crack growth in granular brittle solids. Int. J. of Solids and Structures 115-116, 27–42.

Kuehn, G., Lee, R. W., Nixon, W. A., Schulson, E., 1990. The structure and tensile behaviour of first-year sea ice and laboratory-grown saline ice. J. Offshore Mech. and Arctic Engnin. 112, 357–363.

Kuehn, G., Schulson, E., 1994. The mechanical properties of saline ice under uniaxial compression. Ann. Glaciol. 19, 39–48.

Lee, R., Schulson, E., May 1988. The strength and ductility of ice under tension. J. of Ofshore Mechanics and Arctic Engineering 110, 187–191.

Maus, S., 2020. The plate spacing of sea ice. Annals of Glaciol. 61 (83), 408–425.

Maus, S., Schneebeli, M., Wiegmann, A., 2021. An x-ray micro-tomographic study of the pore space, permeability and percolation threshold of young sea ice. The Cryosphere 15, 4047–4072.
URL https://tc.copernicus.org/articles/15/4047/2021/

Maykut, G. A., 1986. The surface heat and mass balance. Vol. 146 of NATO ASI Series. Plenum Press, Ch. 5, pp. 395–463, ed. by N. Untersteiner.

Michel, B., 1978a. Ice Mechanics. Les Presses De L'Université Laval, Québec, 499 pp.

Michel, B., 1978b. The strength of polycrystalline ice. Can. J. of Civ. Engin. 5 (285-300).

Mullins, W. W., Sekerka, R. F., 1964. Stability of a planar interface during solidification of a dilute binary alloy. J. Appl. Phys. 35 (2), 444–451.

Petrich, C., Eicken, H., 2010. Growth, Structure and Properties of Sea Ice, 2nd Edition. John Wiley and sons, Ch. 2.

Richter-Menge, J. A., Jones, K. F., 1993. The tensile strength of first-year sea ice. J. of Glaciology 39 (133), 609–618.

Sammonds, P. R., Murrell, S., Rist, M., 1998. Fracture of multiyear sea ice. J. Geophys. Res. 103 (C10), 21795–21815.

Schulson, E. M., Duval, P., 2009. Creep and fracture of ice. Cambridge University Press, 401 pp.

Schwarz, J., Weeks, W. F., 1977. Engineering properties of sea ice. J. Glaciol. 19 (81), 499–530.

Shokr, M., Sinha, N., 2015. Sea ice physics and remote sensing. Geophys. Monograph 209. John Wiley and Sons.

Timco, G., Frederking, R., 1986. Confined compression tests: outlining the failure envelope of columnar sea ice. Cold Reg. Sci. and Technol. 12, 13–28.

Timco, G., Weeks, W., 2010. A review of the engineering properties of sea ice. Cold Reg. Sci. Technol. 60, 107–129.

Weeks, W. F., 1961. Studies of salt ice I: The tensile strength of NaCl ice. Crrel research report 80, Cold Regions Research and Engineering Laboratory.

Weeks, W. F., 2010. On Sea Ice. University of Alaska Press.

Weeks, W. F., Ackley, S. F., 1986. The growth, structure and properties of sea ice. In: The Geophysics of Sea Ice. Vol. 146 of NATO ASI Series. Plenum Press, pp. 9–164, ed. by N. Untersteiner.

Weeks, W. F., Assur, A., 1964. Structural control of the vertical variation of the strength of sea and salt ice. Crrel research report 113, Cold Regions Research and Engineering Laboratory.

Weeks, W. F., Hamilton, W. L., 1962. Petrographic characteristics of young sea ice, Point Barrow, Alaska. The Amer. Mineralogist 47, 945–961.

Zhan, C., Sinha, N., Evgin, E., 1996. A three dimensional anisotropic constitutive model for ductile behaviour of columnar sea ice. Acta mater. 44 (5), 1839–1847.